S/5-05

198332

N94-25623

Demonstrating Damage Tolerance of Composite Airframes

C. C. Poe, Jr.
NASA Langley Research Center
Hampton, VA

PAGE_____ INTENTIONALLY BLANK

INTRODUCTION

Commercial transport aircraft operating in the United States are certified by the Federal Aviation Authority to be damage tolerant. On April 28, 1988, Aloha Airlines Flight 243, a Boeing 727-200 airplane, suffered an explosive decompression of the fuselage but landed safely. A photograph of the airplane is shown in Fig. 1. This event provides very strong justification for the damage tolerant design criteria. The likely cause of the explosive decompression was the linkup of numerous small fatigue cracks that initiated at adjacent fastener holes in the lap splice joint at the side of the body. Actually, the design should have limited the damage size to less than two frame spacings (about 40 inches), but this type of "multi-site damage" was not originally taken into account. This cracking pattern developed only in the high-time airplanes (many flights). After discovery in the fleet, a stringent inspection program using eddy current techniques was inaugurated to discover these cracks before they linked up. Because of concerns about safety and the maintenance burden, the lap-splice joints of these high-time airplanes are being modified to remove cracks and prevent new cracking; newer designs account for "multi-site damage".

ALOHA AIRLINES BOEING 737-200

Flight 243, April 28, 1988

Figure 1

APPLICATION OF REGULATIONS TO COMPOSITE AIRCRAFT

Both civil and military regulations are being adapted to composite structures. The source of damage in composite structures is more from accidental impact and lack of adhesion between plies (delamination) than from fatigue. The FAR PART 25 and MIL-STD-1530A implement the guidelines shown in Fig. 2. Both require:

1) ultimate strength and no impairment of function with undetectable impact damage and defects

2) adequate strength to return to base with discrete damage

The military requirement defines detectable impact damage as 0.10-in. or deeper dent; this or a similar requirement will likely be used for civilian airplanes. In the civilian fleet, discrete damage is usually caused by collisions with ground equipment or other airplanes at gates and failure of rotating machinery; in the military fleet, the most critical discrete damage is that caused by weapons.

Computational methodologies or strategies will be illustrated first for discrete damage and then for undetectable impact damage.

FAR PART 25

Withstand ultimate loads with following types of damage: impacts (dropped tools and runway debris), delaminations, surface damage (withstand fatigue loads without growth)

Withstand flight loads with following discrete damage: penetrations over two bays of skin, including one stringer or frame

MIL-STD-1530A

No impairment (repair or water intrusion) after 2 lifetimes with following damage:

tool drop - 0.5" dia. and 6 ft-lbf or visible damage (0.10" dent)

hail - 0.8" dia., SG = 0.9, and 90 ft/s

runway debris - 0.5" dia., SG = 3.0, and appropriate velocity

Adequate strength (consistent with inspectibility) after 2 lifetimes with following damage:

scratch - 0.02" deep and 4.0" long

delamination - equiv. to 2.0" dia. circle with critical shape and location

impact - 1.0" dia. hemispherical tup with 100 ft-lbf or 0.10" dent

Contain battle damage

Figure 2

TENSION DAMAGE TOLERANCE FOR AS4/3501-6

Failing strain is plotted against cut length in Fig. 3 for three structural configurations:

1) a plain composite skin

2) a skin with stiffeners

3) a skin with integral S-glass buffer strips

For the stiffener and buffer strip configurations, respectively, the cut length is equal to two bays of skin and one cut element. The cut length associated with two bays of skin is two times the centerline spacing of stiffeners or two times the centerline spacing of buffer strips less the width of one buffer strip (distance between inside edges rather than between the centerlines). A cut element is a cut stiffener or buffer strip. Cuts can generally be used to conservatively represent discrete damage for uniaxial tension loading. The curves were calculated using linear elastic fracture mechanics and a generalized fracture parameter based on a point strain failure criterion (Refs. 1-7). These predictions are accurate as long as the size of matrix cracks and delaminations at the ends of the cut are small compared to the cut length, much as plastic zone size in homogeneous metals. For long cuts, the curves are linear in the log-log plot with a negative slope of one half. With decreasing cut length, the curves approach the failing strain of the fibers ε_{tuf}, which was calculated as the ratio of unnotched tension strength of the laminate F_{tu} to the Young's modulus in the loading direction E_x. A maximum strain failing criterion is usually quite accurate for laminates with fibers in the loading direction that do not delaminate significantly at the free edges. The two curves, which were calculated for each configuration, represent the range of results for all laminates in the family $0°/\pm45°/90°$ where half of the plies are $\pm45°$. Although the range of failing strains is small, the range of strengths are much larger.

The curves for buffer strips are the highest and those for a plain skin are the lowest; the curves for stiffeners are about midway between. The buffer strips and stiffeners are quite beneficial. The buffer strips are unidirectional strips of S-glass that replace the AS4 fibers in the $0°$ plies. They can be manufactured economically by weaving a largely unidirectional fabric with alternating strips of S-glass and carbon (Ref. 6). The calculations in Fig. 3 were made assuming that the S-glass material has the same thickness as the $0°$ AS4 ply and that the spacing of the buffer strips was five times the width. The failing strain can be increased even more by increasing the thickness and width of the buffer strips. The most effective buffer strip material has the largest product of strength and failing strain. The effectiveness of the stiffeners will be discussed more subsequently.

(See next page for Figure 3)

Design points that represent the regulations in Fig. 2 are also plotted in Fig. 3 for undetectable impact damage and for discrete damage. A design ultimate strain of 0.004 is assumed. The design point for undetectable impact damage is arbitrarily plotted at a cut length of 1 in., which should conservatively represent a 0.10-in. dent caused by an impact; even then, a plain skin is nearly acceptable. Two design points are shown for discrete damage, one for a wing skin and one for a fuselage skin. For a wing, two bays of skin would be about 12 inches (2 × stringer spacing) and, for a fuselage about 40 inches (2 × frame spacing). Following a discrete damage event, FAA Advisory Circular No. 25.571-1A defines ultimate load as "70% of limit maneuver loads and, separately, 40% of limit gust velocity ..., each combined with maximum appropriate cabin differential pressure". Therefore, the strain corresponding to ultimate load for discrete damage would be 70% of 0.004 for the wing and 75% (100/1.33) of 0.004 for the fuselage with cabin pressure alone. For a combination of maneuver loads, gust loads, and cabin pressure, the strain would be between 70 and 75% of 0.004. Skins with buffer strips satisfy the discrete damage criteria for the wing and nearly for the fuselage. Skins with stiffeners alone will nearly satisfy the discrete damage criteria for the wing but not for the fuselage. For buffer strips and stiffeners together, the failing strains may exceed those for buffer strips alone, but that has not been demonstrated. Of course, failing strains can also be elevated by reducing stiffener and buffer strip spacing. Also, matrix cracking at the notch ends may also elevate the failing strains significantly above those plotted in Fig. 3.
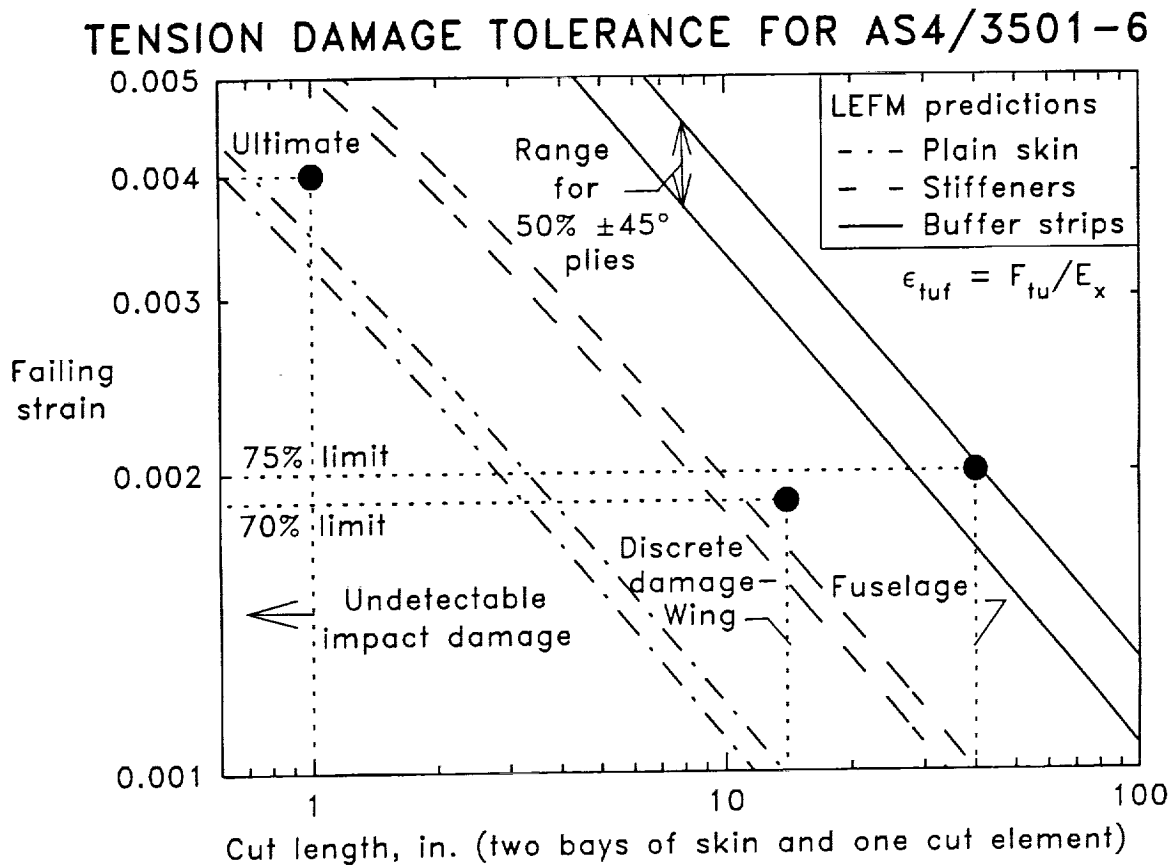

Figure 3

DISCRETE DAMAGE - TOUGH AND BRITTLE RESINS

Strengths normalized by unnotched strengths are plotted against cut length in Fig. 4 for quasi-isotropic laminates made of T300/BP-907 and T300/5208 prepreg tape. The tension strength and failing strain of BP-907 epoxy is more than twice that of 5208, and the matrix damage at the notch tip is accordingly much less. The strengths of the T300/5208 laminates are elevated somewhat relative to those of the T300/BP-907 laminates by the greater matrix damage. The curves are predicted using the same method used in Fig. 3 except that for the T300/5208 laminates, the distance d_0 in the point strain criterion is assumed to increase with increasing cut length to account for matrix damage at the notch tip, which also increases with increasing cut length.

The T300/5208 laminate in Fig. 4 was thin, only 8 plies. Thick (45/0/-45/90) T300/5208 laminates with cuts were shown in Ref. 8 to fail at lower stresses than thin laminates because the notch-tip damage only occurred in the outermost plies. Thus, the damage had negligible effect in thick laminates, and the strengths followed the lower curve in Fig. 4, much like the laminate with BP-907 resin. Also, in Ref. 8, strengths of (0/90) laminates with cuts decreased with increasing thickness, much like the (45/0/-45/90) laminates. On the other hand, the strengths of (0/±45) laminates with cuts increased with increasing thickness. Thus, the predicted strengths in Fig. 3 could be conservative or unconservative due to notch tip matrix damage, depending on layup and thickness. More sophisticated analyses are required to account for notch tip matrix damage.
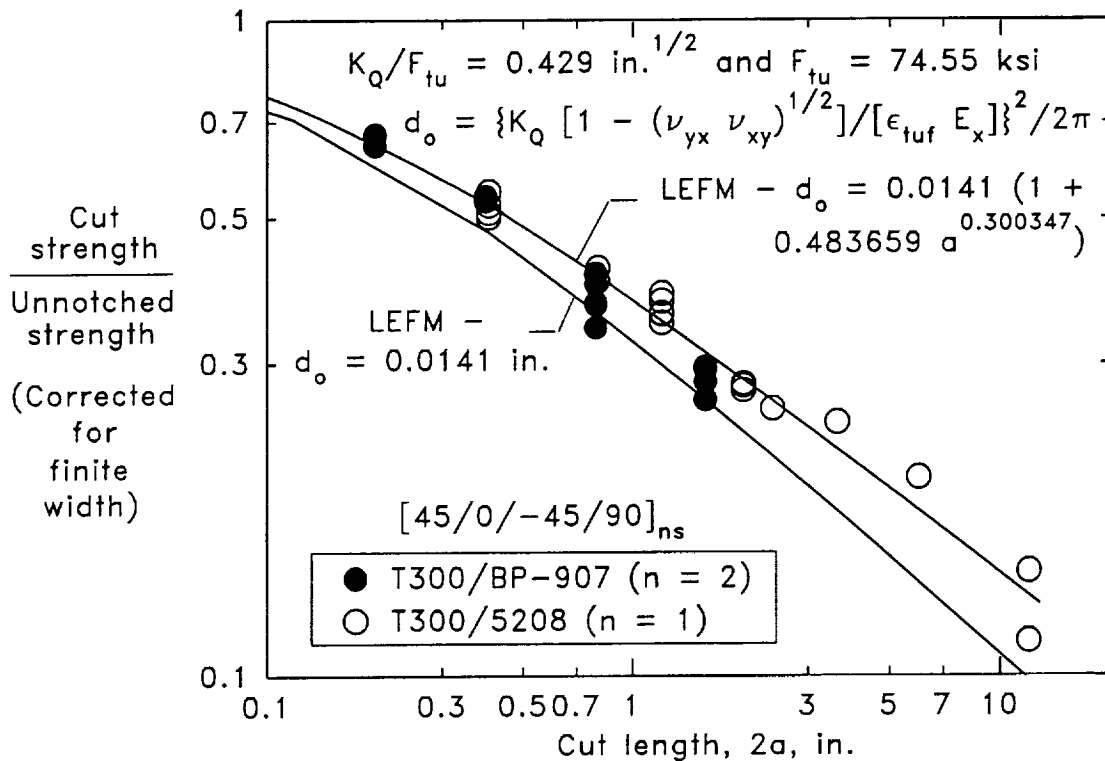

Figure 4

COMPRESSION DAMAGE TOLERANCE FOR HOLES

Little research has been conducted for large discrete damage and compression loading. Nevertheless, some insight can be gained by considering the compression strength of open-hole specimens. Failing strains are plotted against hole diameter in Fig. 5 for 48-ply-thick quasi-isotropic laminates made of T300/5208 prepreg tape (Ref. 9). The test specimens were 5-in. wide. The failing strains were predicted using:

$$\varepsilon_c = \varepsilon_{cu} (1 - 2R/W) K_t^{-1} \tag{1}$$

where ε_{cu} is the unnotched compression failing strain, which was assumed to be 0.014; R is the hole radius; W is the specimen width; and K_t is the stress concentration factor for an isotropic sheet of finite width. For very wide specimens, $K_t = 3$ and the predicting failing strain in Fig. 5 is a horizontal line (0.014/3). For hole diameters greater than 10% of the specimen width, the local stress is elevated by the free edge (finite width effect). The predictions agree with the test data for large holes, but for small holes the test values exceed the predictions because K_t is reduced by matrix cracking at the edge of the hole, which is large compared to hole diameter. If large holes in very wide sheets follow the horizontal line in Fig. 5, failing strains would exceed 0.004. Thus, if discrete damage acts as a large open hole in a very wide sheet, the discrete damage tolerant criterion for the wing should be no more difficult to satisfy for compression loading than for tension loading where strength varies inversely with the square root of damage size. Moreover, stiffeners will have a beneficial effect in compression loading as they did in Fig. 3 for tension loading. On the other hand, buckling could be critical, but no more critical than for metal wings. In the keel area of the fuselage, the compression loads may be significant, and the discrete damage tolerant criterion may be as difficult to satisfy as in the tension case. Complex studies are currently being done in the Advance Composites Technology Program of NASA to develop fuselage and wing structure designs for commercial transport airplanes that satisfy a discrete damage tolerant criterion.
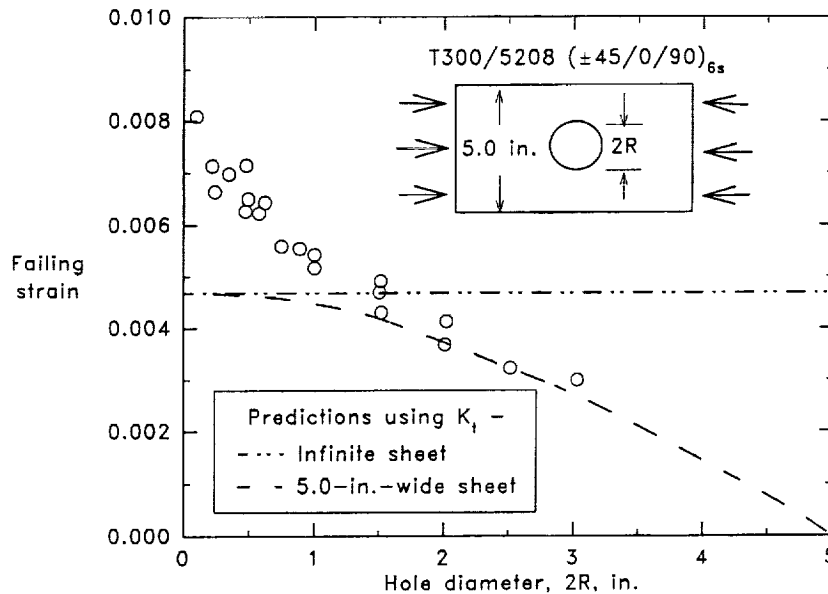

Figure 5

CONFIGURATION OF STIFFENED PANELS

Mechanically attached stiffeners are essential in metal airframe structures to provide damage tolerance with discrete damage. Stringers "pinch" skin cracks when the cracks grow past the stiffeners, reducing the crack tip stresses and elevating the strength (Refs. 10-12). The effectiveness of the stiffeners increases with increasing stiffener stiffness and with decreasing rivet spacing. Integral stiffeners are largely ineffective because the skin crack grows through the stiffener as well as across the skin (Ref. 11).

Stiffened composite panels were fabricated and tested to determine the effectiveness of cocured stiffeners in increasing the residual tension strength of laminates containing a cut (Ref. 7). In contrast to integrally stiffened metal panels, the adhesive bond between the stiffeners and skin is too weak to allow a crack to pass from the skin to the stiffener. The configuration of the panels is shown in Fig. 6. The skin or sheet was made with $(45/0/-45/90)_{2s}$ and $(45/0/-45/0)_{2s}$ layups; the stiffeners, which were unidirectional for simplicity, were made with several widths and thicknesses to give three values of μ, the ratio of stiffener stiffness to panel (total) stiffness. The panels were gripped at the ends to give uniform strain.

Material: T300/5208

Sheet layups: $(45/0/-45/90)_{2S}$

and

$(45/0/-45/0)_{2S}$

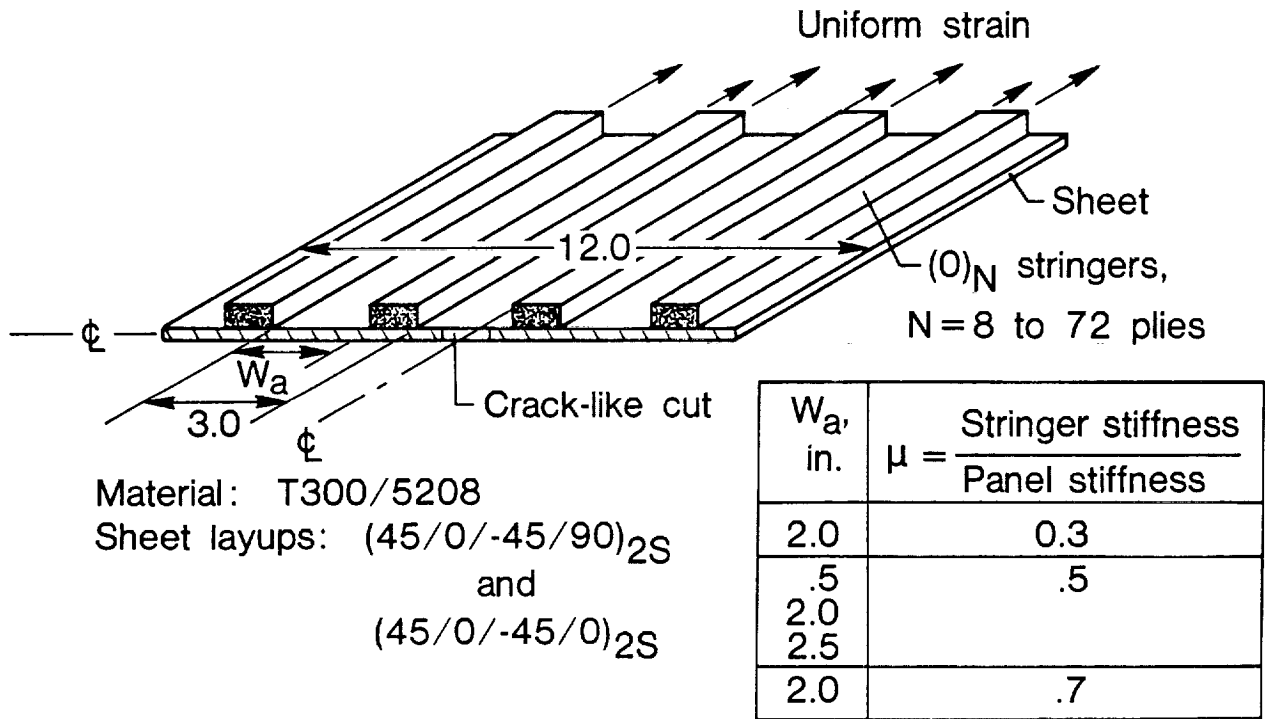| W_a, in.	$\mu = \dfrac{\text{Stringer stiffness}}{\text{Panel stiffness}}$
2.0	0.3
.5 2.0 2.5	.5
2.0	.7

Figure 6

TEST RESULTS FOR (45/0-45/90)2S PANELS WITH μ=0.5

Failing strain is plotted against half-length of crack in Fig. 7 for three of the panels in Fig. 6 with μ=0.5 and quasi-isotropic skins; the panels are labeled A, B and C. The ratio of stringer stiffness to panel stiffness μ was 0.5 for each panel. The width and thickness of the stringers were different for each panel, and the cut lengths increased with decreasing stringer width. A predicted curve is shown for the failing strain of a plain skin. Failure is represented by the small circles labeled A, B and C. Failing strains for the panels with stringers were considerably greater than those predicted for a plain skin. When the applied strains are in the neighborhood of the curve for a plain skin, the cut extends catastrophically but is arrested as the crack grows beneath the stringer. The half-length of the initial cut plus extension is plotted from the abscissa to failure. The extensions were calculated using measurements of crack opening displacement (COD) and assuming that crack length is proportional to COD. The small jumps in crack extension are probably due to damage that develops at the ends of the cuts prior to failure. One radiograph of a crack tip is shown for each panel near failure. Notice that the crack arrests at the near edge of the thinnest stringer but arrests at the far edge of the thickest stringer and arrests between the edges of the stringer with the median thickness. The growth of the cracks beneath the stringers was accompanied by a delamination of the stringers. The delamination reduces the "pinching" effect of the stringers, causing the crack to advance further beneath the stringer. The interlaminar stresses and hence the size of the delaminations increase with increasing crack length and stringer thickness.
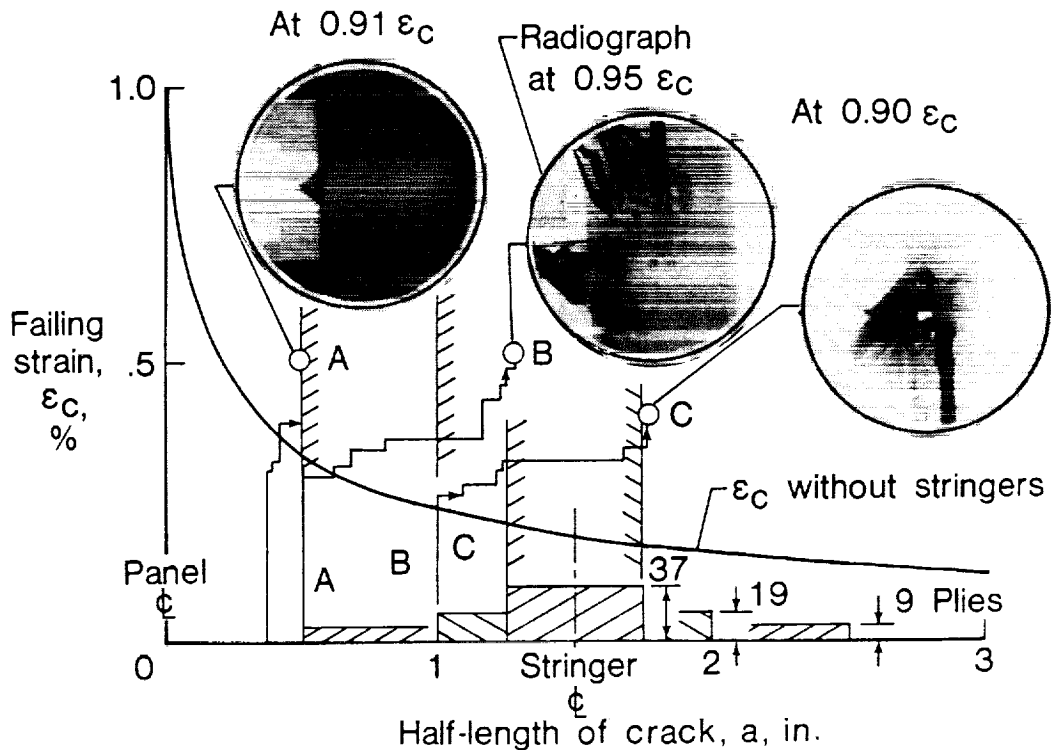

Figure 7

FAILING STRAIN VERSUS STRINGER THICKNESS

Failing strain is plotted against stringer thickness in Fig. 8 for panels in Fig. 6 with $(45/0/-45/90)_{2S}$ and $(45/0/-45/0)_{2S}$ skins. The circular symbols are test results; the solid curves were predicted for the stiffened panels; and the horizontal lines were predicted for plain skins. The predictions for the stiffened panels were made using calculations of stress intensity factors for riveted stringers where rivet spacing was equal to delamination length (Ref. 7). The tests and predictions agree for thin stringers, but the predicted strains are much too large for thick stringers. There was no benefit to increasing stringer thickness much beyond that of skin thickness. The discrepancy between test results and predictions is believed to be due to bending caused by load transferring from the skin to the stringers in the neighborhood of the crack tips. Based on the test results, an appropriate design equation was developed in Ref. 7 that limits the effectiveness of stringers due to bending; this equation was used to make the predictions in Fig. 3. More sophisticated nonlinear analyses are needed to account for bending effects.
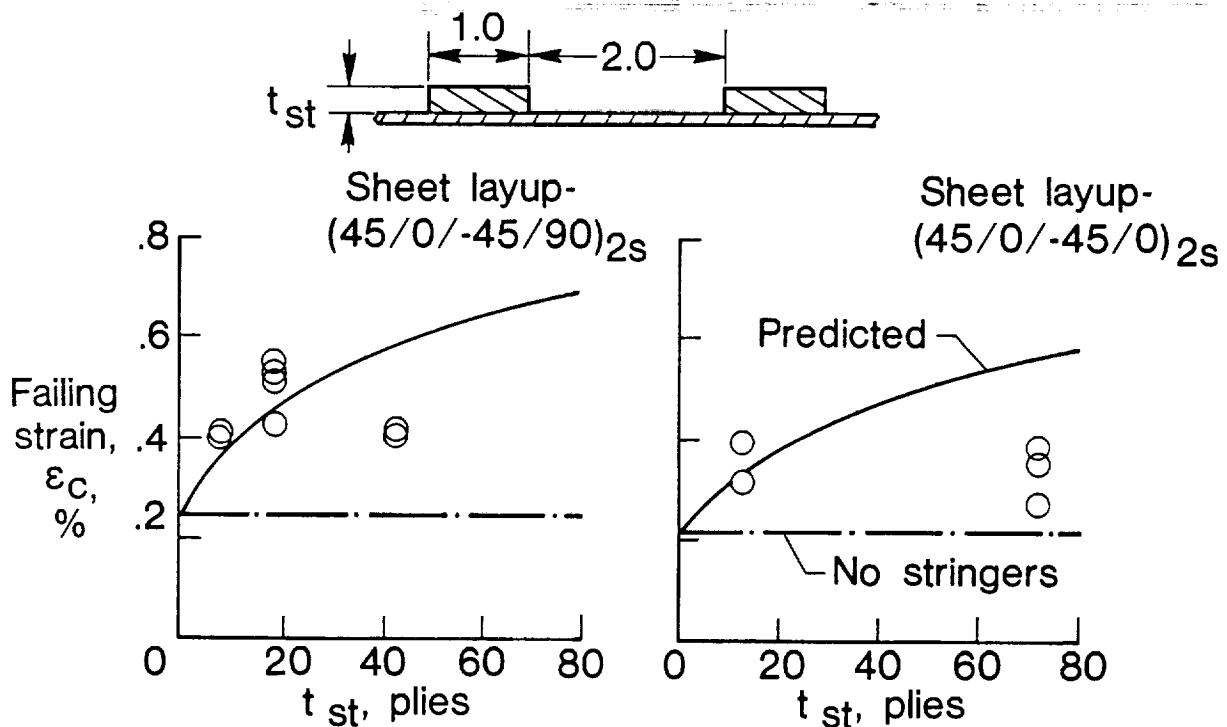

Figure 8

333

CROSS-SECTION OF COMPOSITE AFTER IMPACT
(45/0/-45/90)$_{6s}$ AS4/3501-6

An edge replica of a (45/0/-45/90)$_{6s}$ AS4/3501-6 laminate with impact damage from Ref. 13 is shown in Fig. 9; the cross-section of the 48-ply quasi-isotropic laminate passes through the contact site. The 10.2-lbm impacter had a 0.5-in.-diameter-hemispherical tup attached to the end; the kinetic energy was 20 ft-lbf. The visible damage consists primarily of delaminations and matrix cracks that connect the delaminations in adjacent plies.
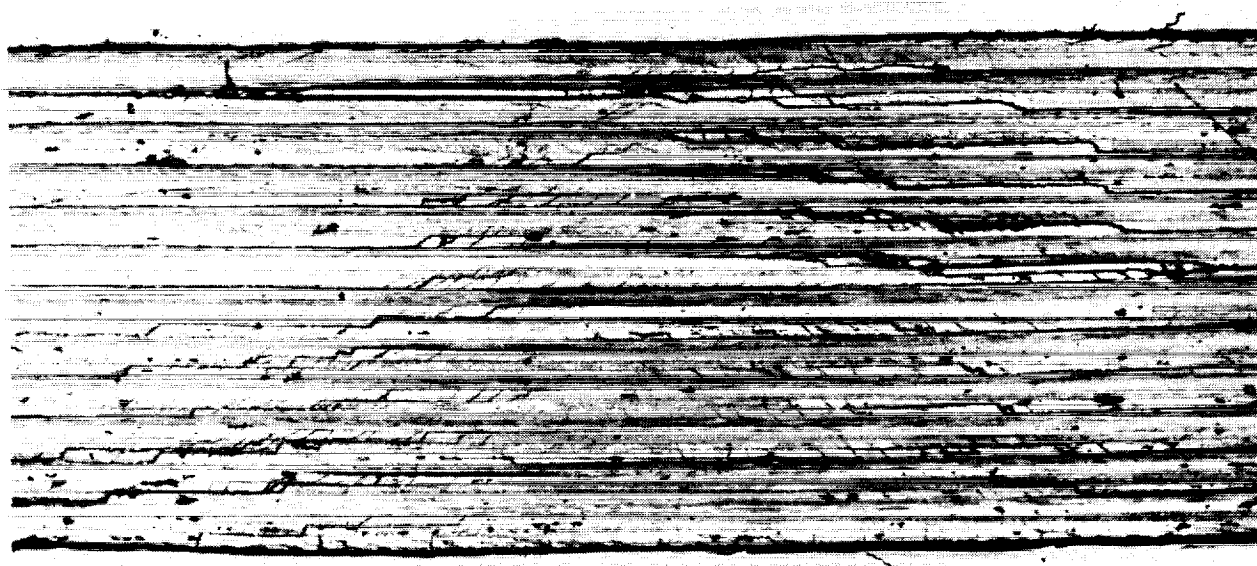

Figure 9

TYPICAL C-SCAN AFTER AN IMPACT

A C-scan of a 48-ply quasi-isotropic laminate with impact damage is shown in Fig. 10. The dark disc in the center of the image indicates delamination damage like that shown in Fig. 9. The delamination between individual interfaces is not a stack of circular discs as suggested by Figs. 9 and 10 but can be represented by spiraling flights of stairs where the stair treads represent delamination (Ref. 14). Two delaminations exist on a given interface; they resemble signal flags on opposite sides of the contact site, initiating at matrix cracks and growing only on one side of the crack (Ref. 15). The C-scan image is circular because it is an average through the thickness.

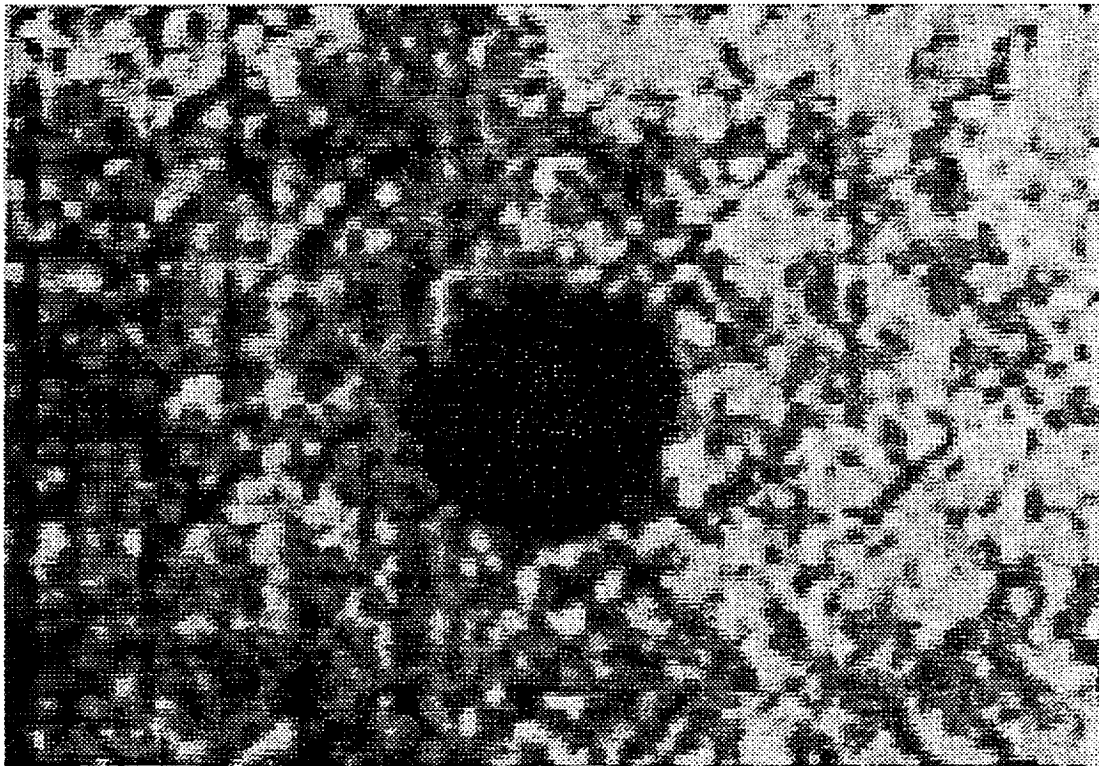# AS4/3501-6 Quasi-Isotropic Laminate

Figure 10

COMPRESSION STRENGTH VERSUS KINETIC ENERGY

Compression strengths with impact damage were measured for quasi-isotropic laminates made with AS4/3501-6 and IM7/8551-7 (Ref. 13); the 3501-6 and 8551-7 resins are brittle and toughened resins, respectively. The compression strengths are plotted against kinetic energy in Fig. 11. The strengths are divided by Young's modulus to give a far-field or remote strain. A Young's modulus of 8 Msi was used for both materials. The impacter had a mass of 10.2-lbm and a 0.5-in.-diameter hemispherical tup. The strengths are reduced dramatically by the impacts; the reduction is significantly more for the brittle resin than for the toughened resin.
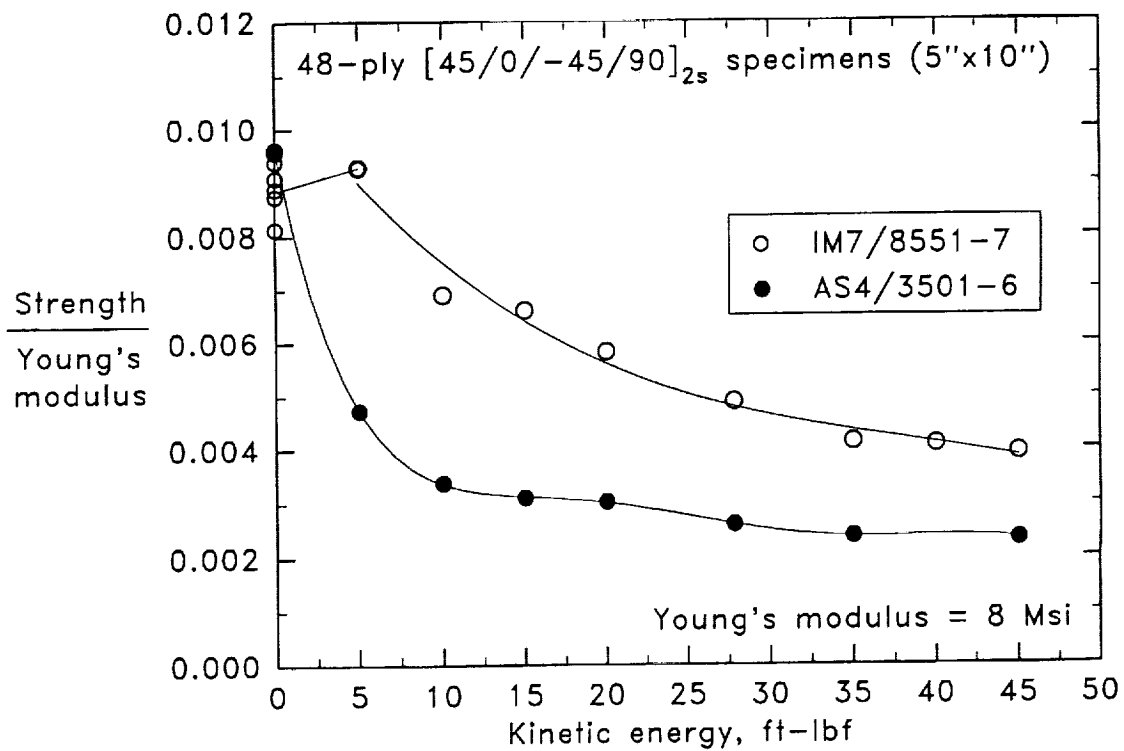
Figure 11

COMPRESSION STRENGTH VERSUS DAMAGE SIZE

The compression strengths divided by Young's modulus in Fig. 11 are replotted against damage diameter in Fig. 12. The damage diameter was calculated from areas of damage in C-scans like that in Fig. 10. For a given kinetic energy, the size of damage for the brittle resin was about two times that for the toughened resin. In terms of damage size, the strengths are nearly equal for the brittle and toughened resins. Thus, the primary difference between the compression strengths of the laminates made with brittle and toughened resins in Fig. 11 is associated with the differences between damage sizes. If damage size and strength are uniquely related, damage size would be a good metric for damage tolerance as well as damage resistance.

The damage diameter associated with the threshold for visible damage is indicated for each material. The failing strain associated with the threshold for visible damage for the toughened 8551-7 resin was significantly greater than 0.004, but that for the brittle 3501-6 resin was slightly below 0.004. The definition of visible damage was subjective and probably represents a dent significantly less deep than 0.1 inches. Thus, both materials may fail to satisfy the undetectable damage criterion for a 0.1-inch deep dent and a design ultimate strain of 0.004.
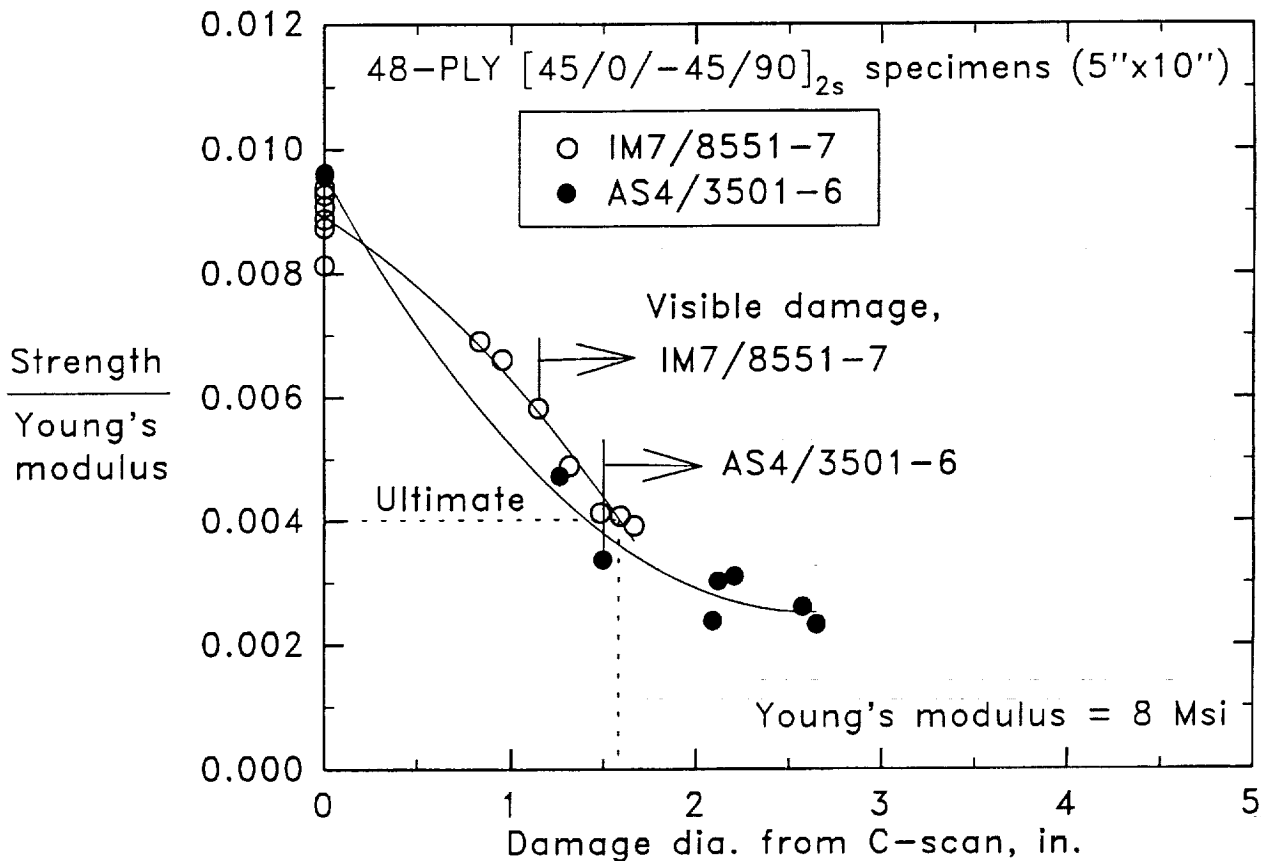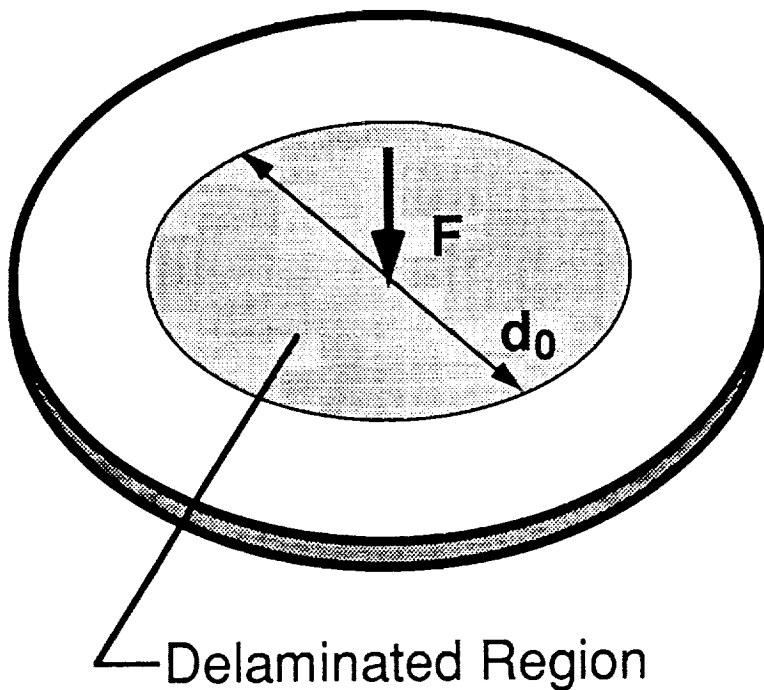
Figure 12

Impact force has been used by numerous investigators (Refs. 13, 15-21) to analyze impact damage like that shown in Figs. 9 and 10. A circular plate impacted at the center with a circular delamination of diameter d_0 is shown in Fig. 13. The force F is the resultant of the contact pressure, which is distributed over the contact diameter. The diameter d_0 is assumed to be large compared to the contact diameter. For an isotropic plate, the problem is symmetric in the polar sense. Neglecting inertial stresses, the transverse shear force per unit width V at the delamination front, which can be obtained solely by equilibrium, is

$$V = F/(\pi d_0) \tag{2}$$

Equation (2) should also be valid for a rectangular plate that is large compared to d_0.

From equilibrium:

$$V = \frac{F}{\pi d_0}$$

Figure 13

CALCULATIONS OF TRANSVERSE SHEAR FORCE

Values of transverse shear force per unit width were calculated for undamaged elastic plates using a dynamic finite element code (Ref. 20). Plate type elements were used to account for flexure of the plate, and a Hertzian spring was used to account for the indentation. The impacter was modeled as a rigid, point mass. The 48-ply-thick, quasi-isotropic square plate was assumed to be made of AS4/3501-6; impacter mass, plate size, and boundary conditions were varied. The kinetic energy and diameter of the impacter was assumed to be 13.6 J and 12.7 mm, respectively. In Fig. 14, peak values of shear force at a distance of 3.18 cm from the center of the plate are plotted against the square root of the frequency ratio $(k/m)^{1/2}/\omega$, where k is the flexural stiffness of the plate; m is the impacter mass; and ω is the first natural frequency of the plate. For a uniformly thick plate, this frequency ratio reduces to the square root of a mass ratio $\alpha(m_p/m)^{1/2}$, where m_p is the mass of the plate and α depends on the boundary conditions. The ordinate is normalized by Eq. (2), where F is the peak force calculated by the finite element code. As the mass of the plate decreases relative to that of the impacter, shear force in Fig. 14 approaches the quasi-static value from Eq. (2). Results for the large plate converge more slowly than those for the small plates and were extrapolated to the static value. These results indicate that the impact can be analyzed quasi-statically if the mass of the impacter is 150 times that of a clamped square plate or 250 times that of a simply supported square plate.
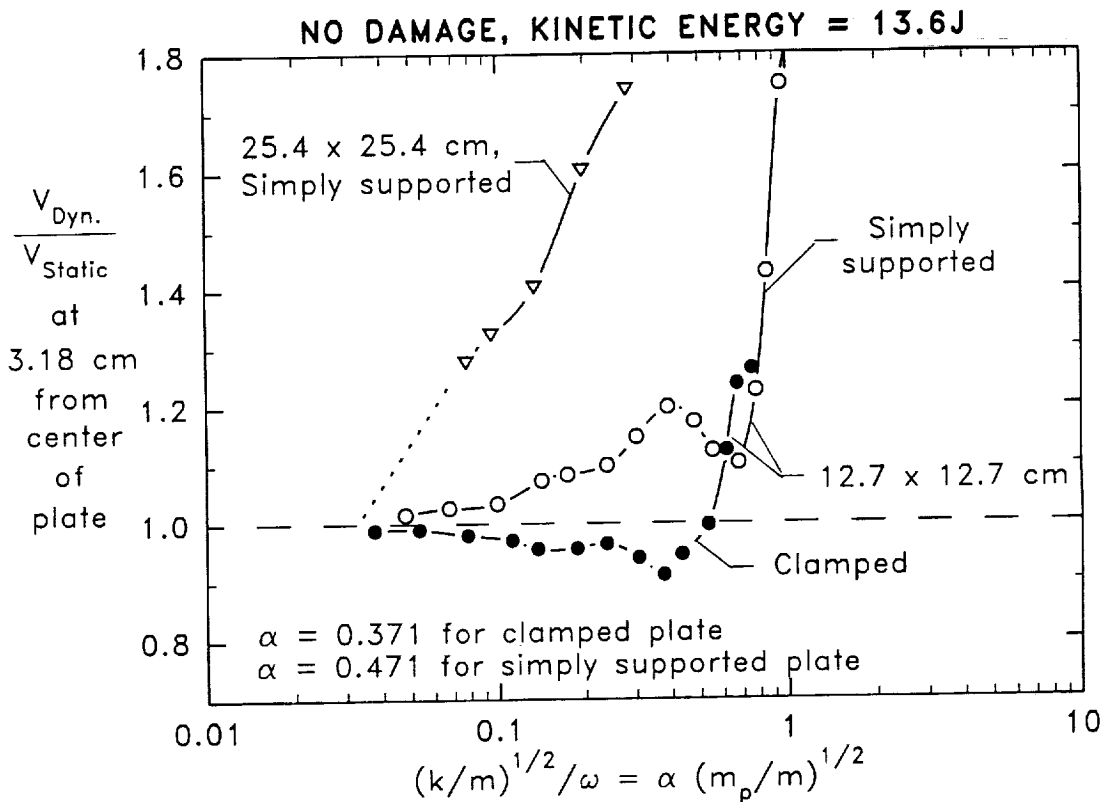

Figure 14

DELAMINATION DIAMETER VERSUS IMPACT FORCE

Values of damage diameter from C-scans are plotted against impact force for static inde;;tation tests and for dynamic impact tests (pendulum) in Fig. 15 (Ref. 21). For the static indentation tests, several plate diameters and two indenter or tup diameters were used. In all cases, the diameters increased in proportion to impact force according to Eq. (2) with V*=41.5 kN/m where the superscript * indicates a critical value of V associated with delamination growth. Thus, V* would make a good metric of damage resistance. Because the size of damage was equal for static indentation and dynamic impact tests, quasi-static behavior is indicated. The value of $\alpha(m_p/m)^{1/2}$ for a 32-ply, 5.08-cm-diameter plate is less than 0.02. Thus, the finite element results in Fig. 14 also predict quasi-static behavior.
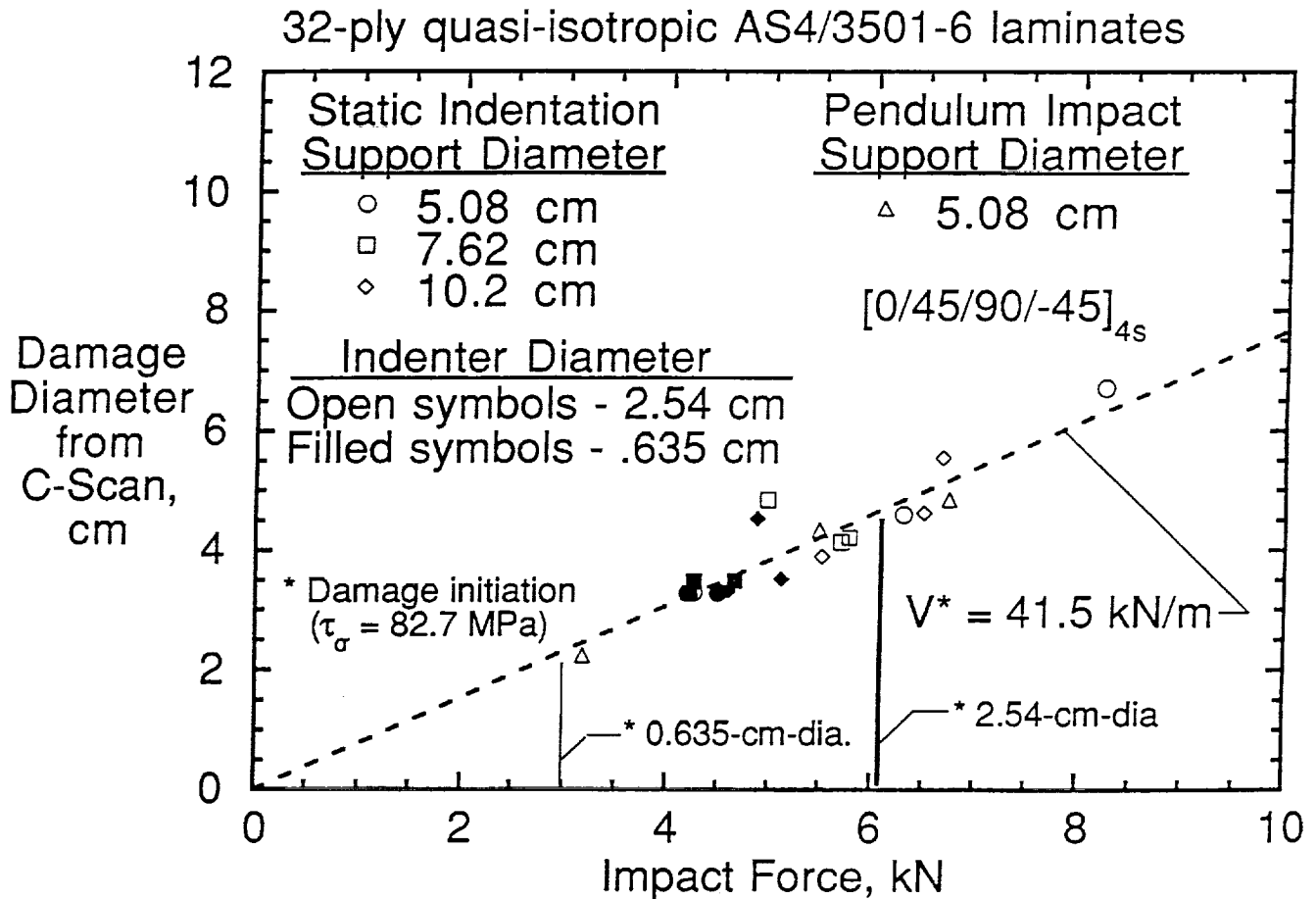

Figure 15

DAMAGE RESISTANCE FOR VARIOUS COMPOSITES

Critical values of transverse shear force are plotted in Fig. 16 for composites with various thicknesses, layups, and resins (Refs. 20 and 21). The 3501-6 epoxy is relatively brittle compared to the 8551-7 which is toughened with an elastomer. For the $\pi/4$ quasi-isotropic (QI) AS4/3501-6 laminates, the resistances for the 6.8- and 7.0-mm-thick laminates are about 85% greater than those for the 3.4- and 4.5-mm-thick laminates. For the 4.5-mm-thick AS4/3501-6 laminates, the resistance for the $\pi/8$-QI laminate is 9% less than that for the $\pi/4$-QI laminate. The resistance for the 7.0-mm-thick $\pi/4$-QI laminate made with 8551-7 is 119% greater than that of the same laminate made with 3501-6. Therefore, thickness and resin toughness had a greater effect on damage resistance than layup.
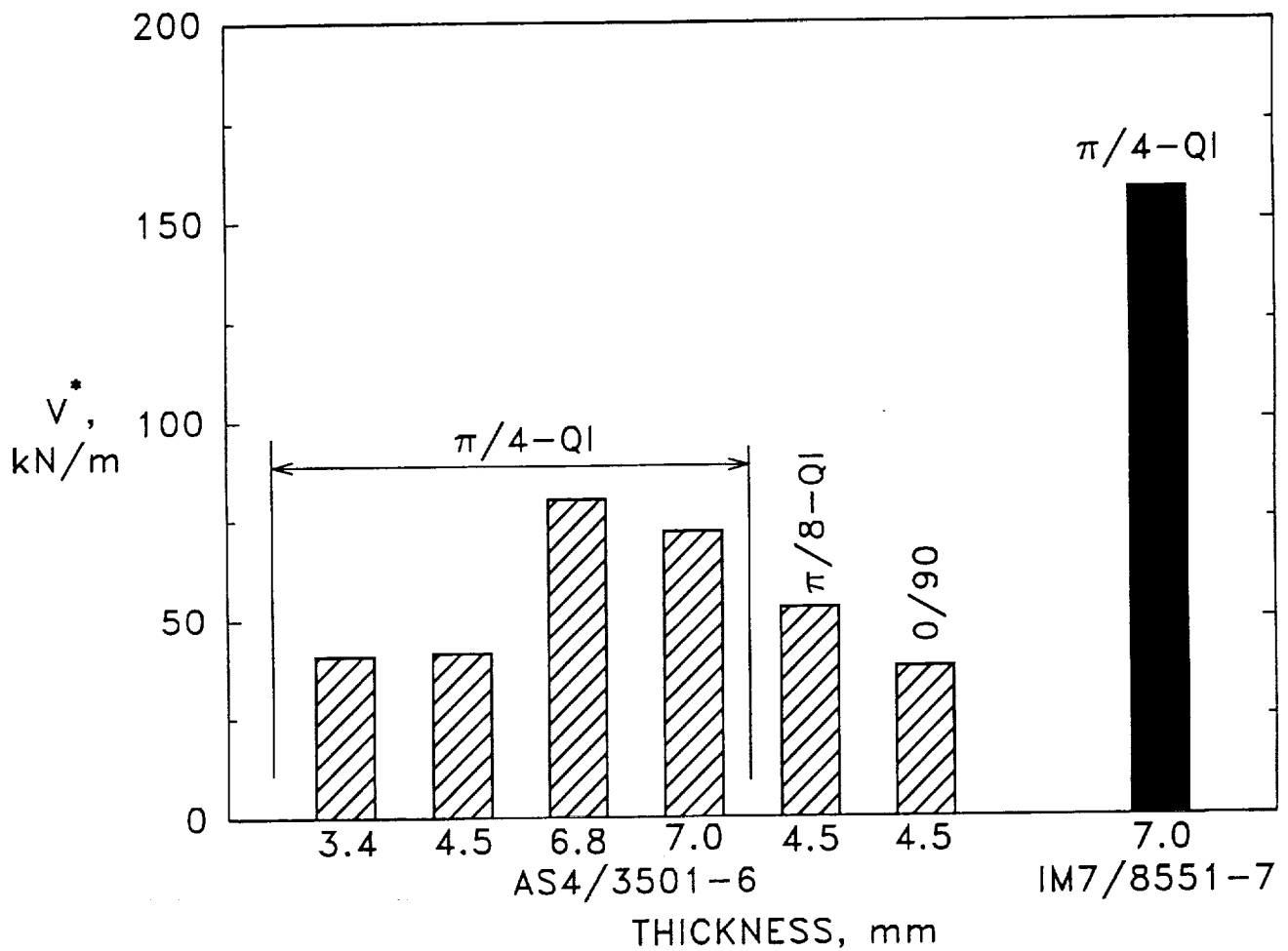

Figure 16

DAMAGE RESISTANCE PREDICTED USING MODE II
STRAIN ENERGY RELEASE RATE

Shivakumar and Elber (Ref. 18) calculated mode I and mode II strain energy release rates for a circular delamination in circular isotropic plates with impact type static loading. The contact pressure was distributed over a constant diameter, and large transverse displacements were taken into account. Mode I values were generally negligible relative to mode II values, which are associated primarily with transverse shear. Values of delamination diameter are plotted against impact force in Fig. 17 for G_{IIc} = 1.5 kJ/m2. The plate thickness was 0.1 cm, the plate radius was 1.27 cm, and the contact radius was 0.05 cm. By using the results for very small impact forces, values of G_{II} were estimated for small displacement theory; then values of delamination diameter were calculated for G_{IIc}=1.5 kJ/m2 and plotted in Fig. 17. A line for V*=53 kN/m was plotted for comparison. For both small and large displacements, the results from Ref. 18 indicate that delamination growth takes place after a critical value of impact force is exceeded. For small displacement theory, the growth is essentially unstable; but, for large displacement theory, the growth is stable as reflected in the test data in Fig. 15. Thus, the large displacement theory is essential to predict damage resistance. Accurate impact damage sizes probably cannot be predicted by modeling the impact damage as a single delamination. Thus, additional analyses are needed for multiple delaminations in anisotropic laminates with noncircular shapes.
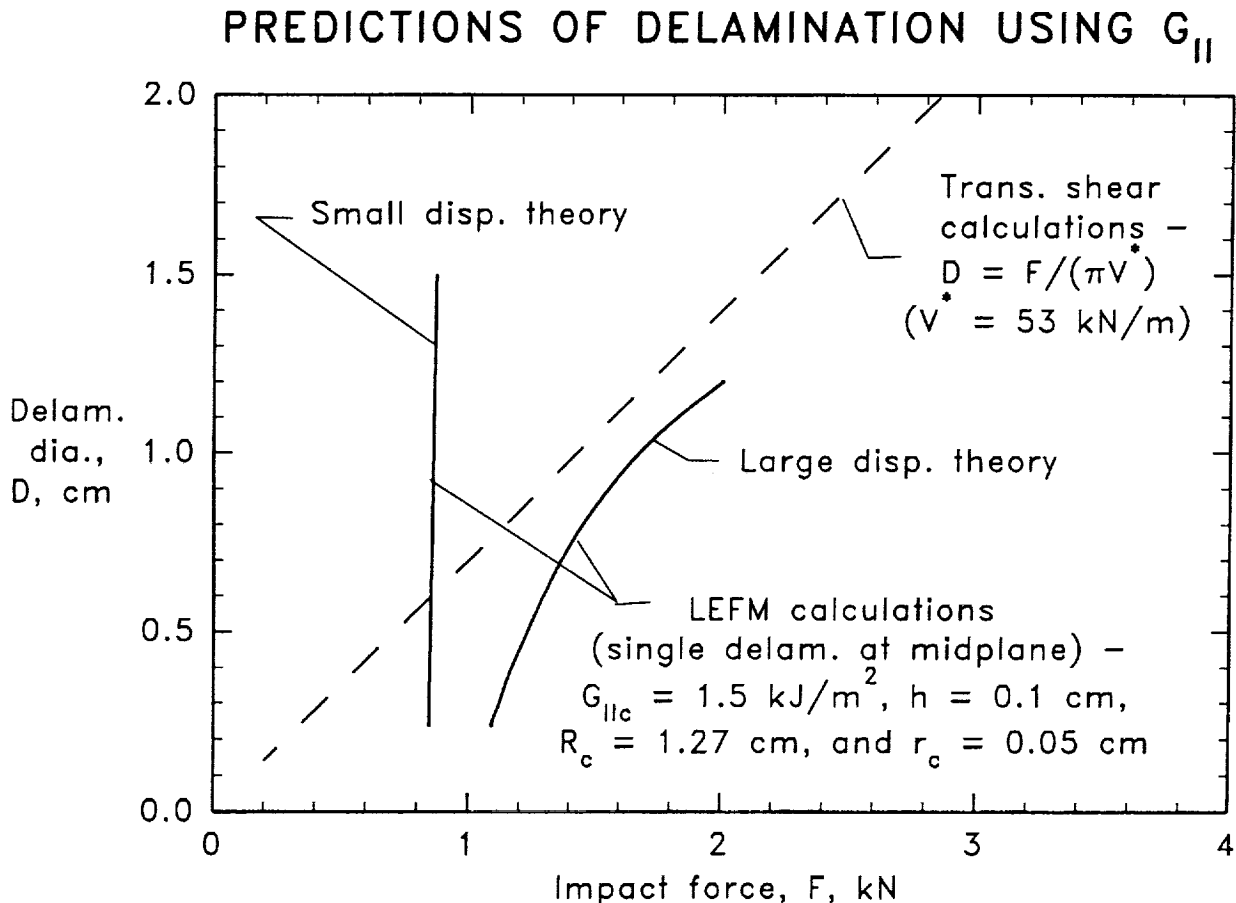

Figure 17

CONCLUSIONS

1. Damage tolerant criteria for civilian airplanes in the United States require ultimate strength with undetectable impact damage and 47 to 50% of ultimate strength (70 to 75% of limit) for discrete damage. Air Force criteria are similar.

DISCRETE DAMAGE

2. For transport airplanes, fuselage is more critical than wing because of larger stiffener spacing.

3. Buffer strips or stiffeners are required.

4. Analyses must account for bending near stiffeners and progressive damage in the skin to make accurate predictions.

5. Methodologies must be developed for compression loads.

UNDETECTABLE IMPACT DAMAGE

6. In plates of 48 plies or less, impact damage consists mostly of ply cracks and delaminations.

7. For a given damage size, compression strengths for toughened and brittle resins are nearly equal.

8. When impacter mass is 150 to 250 times that of the plate, the plate response is quasi-static.

9. Transverse shear force is a metric of damage resistance.

10. Damage resistance increases with increasing resin toughness and plate thickness.

11. Resistance to damage growth may be mostly due to large transverse displacements.

12. A 0.004 ultimate compression strain may not be attainable with a 0.10-in. dent, even for a toughened resin.

REFERENCES

1. Poe, Jr., C. C., "Fracture Toughness of Boron/Aluminum Laminates with Various Proportions of 0° and ±45° Plies," NASA TP-1707, 1980.

2. Poe, Jr., C. C., "A Single Fracture Toughness Parameters for Fibrous Composite Laminates," NASA TM-81911, March 1981.

3. Poe, Jr., C. C., "Fracture Toughness of Fibrous Composite Materials," NASA TP-2370, Nov. 1984.

4. Poe, Jr., C. C., "A Parametric Study of Fracture Toughness of Fibrous Composite Materials," *Journal of Offshore Mechanics and Arctic Engineering*, Vol. 111, No. 3, 1989, pp. 161-169.

5. Poe, Jr., C. C. and Kennedy, John M., "An Assessment of Buffer Strips for Improving Damage Tolerance of Composite Laminates," *Journal of Composite Materials Supplement*, Vol. 14, 1980, pp. 57-70.

6. Kennedy, John M., "Damage Tolerance of Woven Graphite/Epoxy Buffer Strip Panels," NASA TM-102702, Aug. 1990.

7. Poe, Jr., C. C., "Tensile Strength of Composite Sheets with Unidirectional Stringers and Crack-Like Damage - A Brief Report," NASA TM-86310, Sept. 1984.

8. Harris, C. E. and Morris, D. H., "Fracture Behavior of Thick Laminated Graphite/Epoxy Composites," NASA CR-3784, 1984.

9. Rhodes, Marvin D., Mikulas, Jr., Martin M., and McGowan, Paul E., "Effect of Orthotropy and Width on the Compression Strength of Graphite-Epoxy Panels with Holes," AIAA Journal, Vol. 22, No. 9, Sept. 1984, pp. 1283-1292.

10. Poe, Jr., C. C., "Stress Intensity Factor for a Cracked Sheet with Riveted and Uniformly Spaced Stringers," NASA TR-R-358, 1971.

11. Poe, Jr., C. C., "Fatigue Crack Propagation in Stiffened Panels," Damage Tolerance in Aircraft Structures, ASTM STP-486, 1971, pp. 79-97.

12. Poe, Jr., C. C., "The Effect of Broken Stringers on the Stress Intensity Factor for a Uniformly Stiffened Sheet Containing a Crack," NASA TM-X-71947, 1974.

13. Poe, Jr., C. C., Portanova, M. A., Jackson, W. C., Masters, J. E., and Sankar, B. V., "Comparison of Impact Results for Several Polymeric Composites Over a Wide Range of Low Impact Velocities," presented at the First NASA Advanced Composites Technology (ACT) Conference, Seattle, WA, Oct. 30-Nov. 1, 1990; NASA CP-3104, Part 2.

14. Gosse, J. H. and Mori, P. B. Y., "Impact Damage Characterization of Graphite/Epoxy Laminates," in Proceedings of the American Society for Composites, Third Annual Technical Conference, Sept. 25-29, 1988, pp. 344-353.

15. Salpekar, S. A. and O'Brien, T. K., "Analysis of Delamination in Cross Ply Laminates Initiating From Impact Induced Matrix Cracking," NASA CR-187594, Nov. 1991.

16. Greszczuk, L. B., "Damage in Composite Materials Due to Low Velocity Impact," in Impact Dynamics, L. A. Zukas, et al (eds.), John Wiley, New York, 1982, p. 55.

17. Elber, W., "Deformation and Failure Mechanics in Low Velocity Impacts on Thin Composite Laminates," NASA TP-2152, May 1983.

18. Shivakumar, K. N. and Elber, W., "Delamination Growth Analysis in Quasi-Isotropic Laminates Under Loads Simulating Low-Velocity Impact," NASA TM-85819, June 1984.

19. Sjoblom, P. O., Hartness, J. T. and Cordell, T. M., "On Low-Velocity Impact Testing of Composite Materials," Journal of Composite Materials, Vol. 22, Jan. 1988, pp. 30-52.

20. Jackson, W. C. and Poe, Jr., C. C., "The Use of Impact Force as a Scale Parameter for the Impact Response of Composite Laminates," NASA TM-104189, Jan. 1992.

21. Kwon, Y. S. and Sankar, B. V., "Indentation-Flexure Damage in Graphite/Epoxy Laminates," NASA CR-187624, March 1992.

REPORT DOCUMENTATION PAGE

1. AGENCY USE ONLY(Leave blank)	2. REPORT DATE October 1993	3. REPORT TYPE AND DATES COVERED Conference Publication

4. TITLE AND SUBTITLE

Computational Methods for Failure Analysis and Life Prediction

5. FUNDING NUMBERS

WU 505-63-50-17

6. AUTHOR(S)

Ahmed K. Noor, Charles E. Harris, Jerrold M. Housner, and
Dale A. Hopkins, Compilers

7. PERFORMING ORGANIZATION NAME(S) AND ADDRESS(ES)

NASA Langley Research Center
Hampton, VA 23681-0001

8. PERFORMING ORGANIZATION REPORT NUMBER

L-17321

9. SPONSORING/MONITORING AGENCY NAME(S) AND ADDRESS(ES)

National Aeronautics and Space Administration
Washington, DC 20546-0001
and
University of Virginia
Charlottesville, VA 22903-2442

10. SPONSORING/MONITORING AGENCY REPORT NUMBER

NASA CP-3230

11. SUPPLEMENTARY NOTES

12a. DISTRIBUTION/AVAILABILITY STATEMENT

Unclassified–Unlimited

Subject Category 39 and 24

12b. DISTRIBUTION CODE

13. ABSTRACT (Maximum 200 words)

This conference publication contains the presentations and discussions from the joint UVA/NASA Workshop on Computational Methods for Failure Analysis and Life Prediction held at NASA Langley Research Center, October 14–15, 1992. The presentations focused on damage, failure and life predictions of polymer-matrix composite structures. They covered some of the research activities at NASA Langley, NASA Lewis, Southwest Research Institute, industry and universities. Both airframes and propulsion systems were considered.

14. SUBJECT TERMS

Failure analysis; Life prediction; Polymer matrix composites; Computational methods; Airframes; Propulsion systems

15. NUMBER OF PAGES
362

16. PRICE CODE
A16

17. SECURITY CLASSIFICATION OF REPORT Unclassified	18. SECURITY CLASSIFICATION OF THIS PAGE Unclassified	19. SECURITY CLASSIFICATION OF ABSTRACT	20. LIMITATION OF ABSTRACT